

# IMPACT OF THE WIGGLER COHERENT SYNCHROTRON RADIATION IMPEDANCE ON THE BEAM INSTABILITY\*

Juhao Wu<sup>†</sup>, G.V. Stupakov, T.O. Raubenheimer, and Zhirong Huang  
SLAC, Stanford University, Stanford, CA 94309

## Abstract

Previous studies of the (Coherent Synchrotron Radiation) CSR induced longitudinal instability have been made using the CSR impedance due to dipole magnets, however, many storage rings include long wigglers where a large fraction of the synchrotron radiation is emitted. In this paper, the instability due to the CSR impedance from a wiggler is studied assuming a large wiggler parameter  $K$ . The primary consideration is a low frequency microwave-like instability, which arises near the pipe cut-off frequency. Finally, the optimization of the relative fraction of damping due to the wiggler systems is discussed for the damping rings in future linear colliders.

## LONGITUDINAL BEAM INSTABILITY

When the electron bunch passes the curved trajectory inside a dipole, the CSR induces an impedance [1]. The CSR impedance is known to impact single pass bunch compressors where the beam currents are extremely high but it is also possible that CSR might cause a microwave-like beam instability in storage rings. A theory of such an instability in a storage ring has been recently proposed in Ref. [2] where the impedance is generated by the synchrotron radiation of the beam in the storage ring bending magnets. A similar instability may arise due to coherent synchrotron radiation in long wigglers. Many storage rings have used large wiggler systems to reduce the damping times and control the beam emittance. In particular, the high luminosity colliding beam factories, such as DAPHNE, KEK-B, PEP-II, and CESR-C, as well as the damping ring designs for future linear colliders. In a previous study, we have obtained the wakefield and impedance in a wiggler with large parameter  $K$  [3] and, in this paper, we study the impact of the wiggler synchrotron radiation impedance on the beam longitudinal dynamics in rings with dipoles and wigglers.

We will consider the longitudinal dynamics of a thin coasting beam. The beam can be described with a longitudinal distribution function  $\rho(\nu, s, z)$ . The positive direction for the internal coordinate  $s$  is the direction of motion, and  $\nu = (E - E_0)/E_0$ . The position of the reference particle in the beam line is  $z = ct$  with  $c$  the speed of light. We assume that the initial energy distribution function is a Gaussian, i.e.,  $\rho_0 = n_0/(\sqrt{2\pi}\nu_0) \times \exp(-\nu^2/2\nu_0^2)$ , where  $n_0$  is the linear density, i.e., the number of particles per unit length. In this case, the instability is determined by the following dispersion relation [2],

\* The work was supported by the U.S. Department of Energy under Contract No. DE-AC02-76SF00515.

<sup>†</sup> jhwu@SLAC.Stanford.EDU

$$1 = -\frac{i Z(k) \Lambda}{\sqrt{2\pi} k} \int_{-\infty}^{\infty} dp \frac{p e^{-\frac{p^2}{2}}}{\Omega \pm p} \quad (1)$$

where,  $\omega$  and  $k$  are the perturbation frequency and wavenumber respectively;  $\Lambda = n_0 r_0 / (|\eta| \gamma \nu_0^2)$ ;  $\Omega = \omega / (ck|\eta|\nu_0)$ ;  $p = \nu/\nu_0$ ;  $\eta$  is the slippage factor and  $r_0 \approx 2.82 \times 10^{-15}$  m is the classical electron radius and  $\gamma$  is the Lorentz factor. In addition,  $Z(k) = \int_0^{\infty} ds w(s) \exp\{-iks\}$ , is the CSR impedance and  $w(s)$  is the wake Green function.

	NLC	TESLA	ATF
Circumference $C/\text{km}$	0.3	17	0.14
Dipole radius $R/\text{m}$	5.5	80	5.7
Total bending angle $\Theta/2\pi$	1	5/3	1
Moment. comp. $\alpha/10^{-4}$	2.95	1.2	19
Energy $E/\text{Gev}$	1.98	5	1.3
Energy rms spread $\nu_0/10^{-4}$	9.09	9	6
Bunch rms length $\sigma_z/\text{mm}$	3.6	6	5
Particles per bunch $N_e/10^{10}$	0.75	2	1
Wiggler peak field $B_w/\text{T}$	2.15	1.5	1.88
Wiggler period $\lambda_w/\text{m}$	0.27	0.4	0.4
Wiggler total length $L_w/\text{m}$	46.24	432	21.2
Pipe radius $b/\text{cm}$	1.6	2	1.2
$F_w$	2.2	13.4	1.8
Cut-off wavelength $\lambda_c/\text{mm}$	4.9	1.8	3.1
Threshold (off) $N_t/10^{10}$	0.60	27.44	0.95
Threshold (on) $N_t/10^{10}$	0.52	24.56	0.76
Growth time (off) $\tau/\mu\text{s}$	54.9	N/A	34.3
Growth time (on) $\tau/\mu\text{s}$	32.9	N/A	6.5

Table 1: Parameters and results.

## STORAGE RINGS WITH WIGGLERS

As concrete examples, we study the NLC main damping ring [4], the TESLA damping ring [5], and the KEK ATF prototype damping ring [6]. Parameters are given in Table 1. In our model, we use the steady state CSR impedance and assume a distributed model. For a dipole, the steady state CSR impedance is [1]:  $Z_D(k) = -i A k^{1/3} R^{-2/3}$ , with  $A = 3^{-1/3} \Gamma(2/3) (\sqrt{3}i - 1) \approx -0.94 + 1.63i$ . The wiggler impedance  $Z_W(k)$  is computed in Ref. [3]. Hence, the total impedance is then:  $Z(k) = Z_D(k) \Theta R/C + Z_W(k) L_W/C$ , where,  $R$ ,  $\Theta$ ,  $L_W$  and  $C$  are the dipole bending radius, the total bending angle, the wiggler total length and the damping ring circumference given in Table 1 respectively. To study the instability, we numerically solve the dispersion relation Eq. (1). In Fig. 1, the imaginary part of  $\Omega$  is plotted as a function of the instability wavenumber

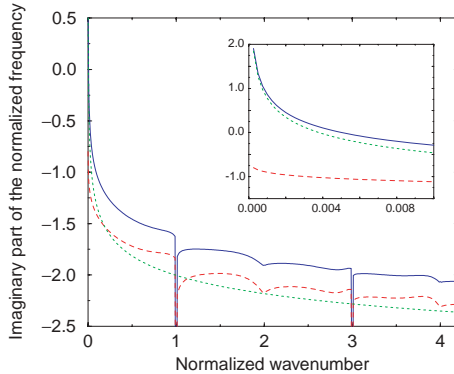


Figure 1: The imaginary part of the normalized frequency  $\Omega$  as a function of the normalized wavenumber  $k/k_0$  for the NLC main damping ring [4]. The solid curve includes the entire CSR impedance while the dotted and dashed curves include either the steady state dipole CSR impedance or the wiggler CSR impedance, respectively. The inset shows a blow up of the low frequency unstable region.

for the NLC main damping ring using the parameters listed in Table 1. At low frequencies, the dipole CSR impedance dominates while at shorter wavelengths the wiggler CSR impedance is usually more important. In the region where  $\text{Im}(\Omega) < 0$ , the beam is stable and this is true for all regions except at the longest wavelengths as shown in the inset. This low frequency instability will be discussed subsequently. Based on similar calculations, we find that with the design current in the TESLA damping ring, the impedance from the dipoles and wigglers will not drive an instability while the results for the ATF are very similar to those of the NLC damping ring shown in Fig. 1.

As seen in Fig. 1, the instability is most important at relatively low frequency. We can use a simple scaling analysis to understand this. The dipole CSR impedance scales as  $Z_D(k) \propto k^{1/3}$ . Similarly, the low frequency behavior of the wiggler impedance is [3]:  $Z_W(k) = \pi k_w(k/k_0)[1 - (2i/\pi)\log(k/k_0)]$ ; which is accurate for  $k \in [0, 0.1 k_0]$ , where  $k_0 = 2\gamma^2 k_w/(1 + K^2/2)$  is the wiggler fundamental radiation wavenumber and the wiggler parameter  $K \approx 93.4 B_w \lambda_w$ , with  $B_w$  the peak magnetic field of the wiggler in units of Tesla and  $\lambda_w$  the period in meters. Thus, the wiggler CSR impedance scales as  $\text{Re}[Z_W(k)] \propto k$ , and  $\text{Im}[Z_W(k)] \propto k \log(k)$ , which is a weaker scaling than  $k$  over the range of interest. Hence, the CSR induced energy modulation has a scaling no-stronger than  $k$ . On the other hand, the Landau damping due to the phase mixing is more serious for short wavelength perturbations and the resulting damping is proportional to  $k$ . Since the growth due to the CSR impedance is weaker than the linear scaling of the phase mixing effect, it is expected that the threshold is determined by the perturbation with the longest wavelength.

The vacuum chamber causes an exponential suppression of the synchrotron radiation at wavelengths  $\lambda$  greater than the ‘shielding cutoff’ [7]  $\lambda_c \leq 4\sqrt{2}b(b/R)^{1/2}$ . Here,  $R$  is

the dipole bending radius, and  $b$  is the vacuum chamber half height. We assume that the vacuum chamber is made up of two infinitely wide plates. Given the previous discussion, the threshold will be the lowest at the smaller of the bunch length or the ‘shielding cutoff’ wavelength.

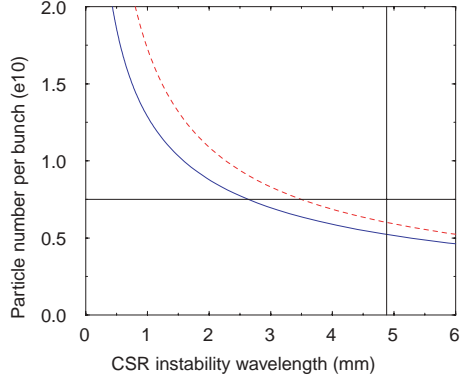


Figure 2: The threshold as a function of the CSR wavelength for the NLC main damping ring. The dashed curve is the result for the dipoles only; the solid curve for both the dipoles and the wigglers. The vertical straight line is the approximate cutoff wavelength; the horizontal straight line is the nominal number of particles per bunch:  $0.75 \times 10^{10}$ .

For the NLC main damping ring, we find that perturbations with wavelengths  $\lambda > 3.5$  mm are not stable due to the dipole CSR impedance alone. Adding the CSR impedance from the wiggler causes perturbations with wavelengths  $\lambda > 2.6$  mm to be unstable. In Fig. 2, the threshold particle number is plotted as a function of the perturbation wavelength. Next, in Fig. 3, the growth time,  $\tau \equiv (\text{Im}(\Omega)ck|\eta|\nu_0)^{-1}$ , is plotted versus the perturbation wavelength. It is clearly seen that the threshold current decreases as we approach the longer wavelength perturbations as expected from our scaling analysis. Based on the parameters in Table 1, the ‘shielding cutoff’ wavelength is  $\lambda_c \approx 4.9$  mm. At this cutoff wavelength, the threshold currents and growth time are summarized in Table 1. The growth time is significantly faster than the synchrotron period, in consistent with the analysis for a microwave-like instability.

For the KEK ATF prototype damping ring, the cut-off wavelength would be about  $\lambda_c \approx 3.1$  mm. Taking the dipole CSR impedance alone, the instability sets in for perturbations with wavelengths  $\lambda > 2.8$  mm. Adding the wiggler CSR impedance, the electron beam would be unstable for perturbations with wavelengths  $\lambda > 1.9$  mm. Other results are summarized in Table 1.

It is interesting to note that in both the NLC and the ATF damping rings roughly twice as much synchrotron radiation power is emitted in the wiggler as in the arc dipoles. However, the instability threshold is not dramatically impacted by the additional radiation and decreases by less than a factor of two in each case. This arises because of the very different low frequency scaling of the impedances. It

also suggests an optimization of the damping ring design where a larger fraction of radiation is emitted in the wigglers as will be discussed subsequently.

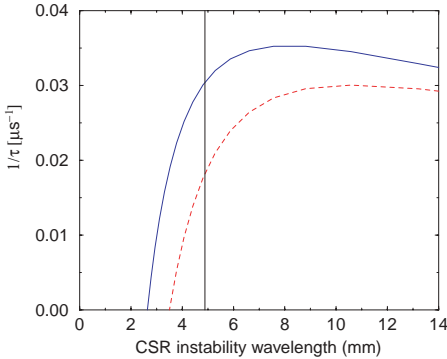


Figure 3: The growth rate as a function of the CSR wavelength for the NLC main damping ring. The dashed curve is the result for the dipoles only; the solid curve for both the dipoles and the wigglers. The vertical straight line is the approximate cutoff wavelength.

## DAMPING RING OPTIMIZATION

To study the ring optimization, we use expressions derived in Ref. [8] for the damping ring parameters. The primary constraint is the damping times. Because all linear collider designs presently only consider flat beams with  $\sigma_x \gg \sigma_y$ , the tightest requirement is on the vertical damping time which, using Eq. (11) of Ref. [8], can be written  $\tau_y \approx ((2.89 \times 10^{12} \text{kG})C|\Theta| / (|B_a|\gamma^2(1+F_w)c2\pi))$ , where  $B_a$  is the arc bending field,  $C$  is the ring circumference,  $\Theta$  is the total bending angle of the arcs, and  $F_w$  is defined as the ratio of the damping due to the wiggler over the damping due to the arc bending magnets:  $F_w \equiv I_{2w}/I_{2a}$ . Here,  $I_{2a}$  and  $I_{2w}$  are the second synchrotron integrals calculated over the arcs and the wigglers respectively.

Since  $B_a \propto 1/(1+F_w)$ , for a given ring size and damping time and, given a maximum wiggler field, the required wiggler length can be found. At this point, we can calculate the other ring parameters. According to the dispersion relation in Eq. (1), we will need the momentum compaction factor  $\alpha$ , the energy spread  $\nu_0$ , and the bunch rms length  $\sigma_z$ . Using Eqs. (37), (39) and (40) from Ref. [8], the scaling can be written:  $\alpha \propto (1+F_w)^{5/3}$ ,  $\nu_0 \propto \sqrt{(B_a + B_w F_w)/(1+F_w)}$ , and  $\sigma_z \propto \nu_0 \sqrt{\alpha}$ . Using these relations, we estimated parameters for NLC ring with  $F_w = 0$  and  $F_w = 6.5$ . These parameters are summarized in Table II along with the nominal  $F_w = 2.2$ .

At this point, we can study the threshold. Based on our previous studies, we expect the CSR impedance from the wiggler to be small compared to the CSR impedance of dipoles in the low frequency region of interest. Hence,

the threshold is essentially determined by the dipole CSR impedance. According to the dipole CSR impedance, and the relation between  $B_a$  and  $F_w$ , the total impedance should scale as  $Z(k) \propto Z_D(k)R \propto R^{1/3} \propto (1+F_w)^{1/3}$ , at a fixed wavenumber  $k$ . Clearly, this is an increasing function with  $F_w$  however, according to the dispersion relation in Eq. (1), the threshold will scale as:  $N_t \propto \alpha \nu_0^2 \sigma_z / Z(k) \propto (1+F_w)^{13/6}$ , where it was assumed that  $B_a \sim B_w$ , so  $\nu_0$  is roughly constant. Thus, it is expected that increasing  $F_w$  will increase the threshold significantly. In addition, the cutoff wavelength  $\lambda_c$  scales as  $R^{-1/2}$ , i.e. scales as  $(1+F_w)^{-1/2}$  and the cutoff wavelength will decrease as  $F_w$  increases and  $B_a$  decreases. Since, the threshold is lowest at long wavelength, the threshold will increase as  $F_w$  is increased due to both the shift in the cutoff wavelength as well as the change in the ring parameters. The above scaling analysis has been compared to numerical calculations for the NLC damping ring. The results are given in Table 2. Clearly, the threshold increases rapidly as  $F_w$  is increased as expected. Integrated with other considerations [9], the result here led to a redesign for the NLC damping which increases the threshold to more than four times the nominal charge per bunch [10].

$F_w$	0	2.2	6.5
Dipole field $B_a/\text{T}$	3.8	1.2	0.55
Dipole radius $R/\text{m}$	1.7	5.5	12.0
Wiggler length $L_w/\text{m}$	0	46.24	66
Momentum compaction $\alpha/10^{-4}$	0.69	2.95	14
Energy rms spread $\nu_0/10^{-4}$	13	9.09	8.4
Bunch rms length $\sigma_z/\text{mm}$	2.4	3.6	5.5
Cutoff wavelength $\lambda_c/\text{mm}$	8.7	4.9	3.3
Threshold at cutoff $N_t/10^9$	2.0	5.2	31.3

Table 2: Parameters and results for the NLC main damping ring when  $F_w=0, 2.2$  and  $6.5$ .

## REFERENCES

- [1] J.B. Murphy, S. Krinsky, and R.L. Gluckstern, Part. Accel. **57**, 9 (1997).
- [2] G. Stupakov, S. Heifets, Phys. Rev. ST Accel. Beams **5**, 054402 (2002).
- [3] J. Wu, T.O. Raubenheimer, G.V. Stupakov, Phys. Rev. ST Accel. Beams **6**, 040701 (2003).
- [4] A. Wolski, URL: <http://awolski.lbl.gov/nlcdrlattice/default.htm>.
- [5] W. Decking, "The TESLA Damping Ring", in *Snowmass 2001*, July 2001.
- [6] <http://www-jlc.kek.jp/atf/ATF.overview-e.html>.
- [7] R.L. Warnock and P. Morton, Part. Accel. **25**, 113 (1990).
- [8] P. Emma, T. Raubenheimer, Phys. Rev. ST Accel. Beams **4** 021001 (2001).
- [9] M. Venturini, "Wigglers and Single-Particle Dynamics in the NLC Damping Rings", these proceedings.
- [10] A. Wolski *et al.*, "A Lattice With Large Momentum Compaction for the NLC Main Damping Rings", these proceedings.